

MISR Photogrammetric Data Reduction for Geophysical Retrievals

Veljko M. Jovanovic, Michael M. Smyth, Jia Zong, Robert Ando, and Graham W. Bothwell

Abstract— The theoretical concept, based on modern photogrammetric methods, underlying the design of the Multi-angle Imaging SpectroRadiometer (MISR) science data processing system, responsible for the autonomous and continuous georectification of multiangle imagery, is the subject of this paper. The algorithm partitions effort between the MISR Science Computing Facility and the Earth Observing System (EOS) Distributed Active Archive Center (DAAC) in a way that minimizes the amount of processing required at the latter location to rectify and map project remotely sensed data online, as it comes from the instrument. The algorithm deals with the following issues:

- 1) removal of the errors introduced by inaccurate navigation and attitude data;
- 2) removal of the distortions introduced by surface topography;
- 3) attainment of a balance between limited hardware resources, huge data volume and processing requirements, and autonomous and nonstop aspects of the production system.

Index Terms— Calibration, mapping, photogrammetry, rectification.

I. INTRODUCTION

THE MULTI-angle Imaging SpectroRadiometer (MISR) is part of the Earth Observing System (EOS)-AM1 payload to be launched in 1998 [3]. The purpose of MISR is to study the ecology and climate of the earth through the acquisition of systematic, global, multiangle imagery in reflected sunlight. In order to derive geophysical parameters, such as aerosol optical depth, bidirectional reflectance factor, and hemispheric reflectance, measured incident radiances from the multicamera instrument must be coregistered. Furthermore, the coregistered image data and any subsequently derived product (e.g. cloud-top heights) must be geolocated to meet experiment objectives, such as: a) producing a data set of value to long-term monitoring programs and allowing intercomparisons of data on time scales exceeding that of an individual satellite and b) providing EOS synergism by allowing data exchange between EOS platform instruments.

The requirements for coregistration and geolocation (i.e., orthorectification) as well as stereo retrieval of a surface height from multitemporal, multiangle image data has been recognized since the early days of remote sensing. In order to

do this, geometric distortions must be removed. The distortions are related to a number of factors, including the following:

- 1) rotation of the earth during image acquisition;
- 2) finite scan rate of some sensors;
- 3) wide field-of-view of some sensors;
- 4) curvature of the earth;
- 5) sensor nonidealities;
- 6) variations in platform altitude, attitude, and velocities;
- 7) panoramic and topographic effects related to the imaging geometry.

A number of methods have been used to remove these distortions, from the simplest image-warping techniques known as “rubber sheeting” to the rigorous implementation of imaging geometry, including a camera geometric model. In most applications, the geometric data correction is not part of standard processing. Usually, standard digital data products have been only radiometrically and spectrally corrected before being distributed to investigators, who may then need to build an offline geometric processing system [2].

In the case of the spaceborne MISR instrument with its unique configuration of nine fixed pushbroom cameras, continuous and autonomous coregistration and geolocation of the image data are required prior to application of scientific retrieval algorithms. To address this problem, the MISR ground data processing system includes geometric processing. The algorithms used are based on modern digital photogrammetry methods. This paper describes an integrated process using techniques, including the following:

- 1) area-based/feature-based image matching;
- 2) image point intersection;
- 3) space resection;
- 4) simultaneous bundle adjustment;
- 5) image-to-image registration in support of MISR systematic data processing.

Section II describes the geometry of the MISR instrument. Section III describes the data products produced by standard data processing using photogrammetry-based algorithms. The remaining sections describe the theoretical concepts underlying the algorithms.

II. GEOMETRY OF THE MISR IMAGING EVENT

The baseline orbit for the EOS-AM1 spacecraft has been selected by the EOS project to be sun-synchronous, with an inclination of 98.186° . The orbit period of 98.88 min and orbit precession rate of $0.986^\circ/\text{day}$ imply a ground repeat cycle of the spacecraft nadir point of 16 days. The orbit altitude

Manuscript received November 4, 1997; revised February 26, 1998. This work is supported by the Jet Propulsion Laboratory, California Institute of Technology, under contract with the National Aeronautics and Space Administration.

The authors are with the Jet Propulsion Laboratory, California Institute of Technology, Pasadena, CA 91109 USA (e-mail: vmj@jrd.jpl.nasa.gov).

Publisher Item Identifier S 0196-2892(98)04749-4.

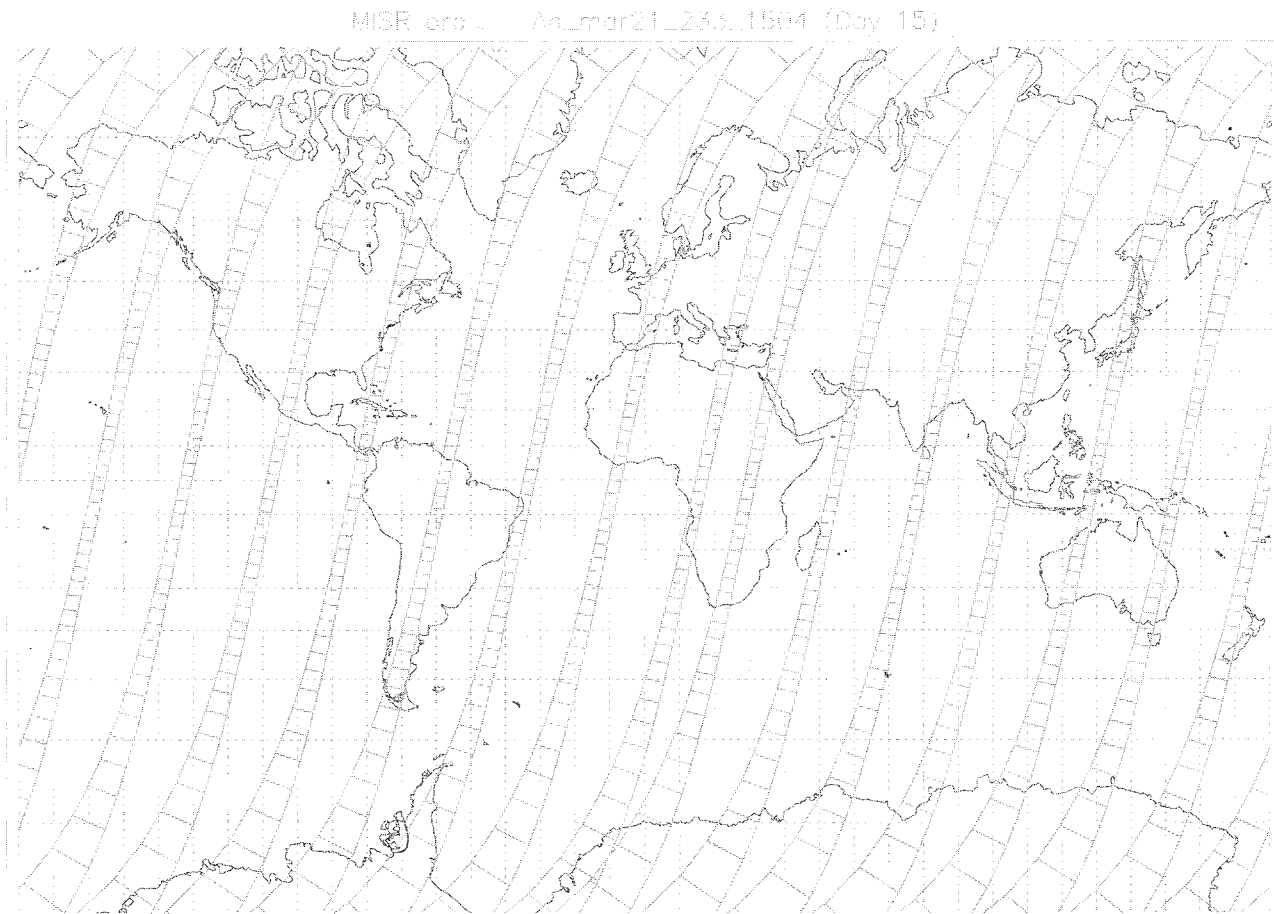


Fig. 1. MISR nominal ground coverage during a one-day period. There are 16 ground tracks obtained by projecting IFOV for the nadir camera.

varies from about 704 km to a maximum of 730 km. The orbit will have an equatorial local crossing time of 10:30 a.m. Fig. 1 shows MISR nominal ground coverage during a one-day period.

The MISR instrument consists of nine pushbroom cameras. The cameras are arranged with one camera pointing toward the nadir (designated An), one bank of four cameras pointing in the forward direction (designated Af, Bf, Cf, and Df in order of increasing off-nadir angle), and one bank of four cameras pointing in the aftward direction (using the same convention but designated Aa, Ba, Ca, and Da). Images are acquired with nominal view angles, relative to the surface reference ellipsoid, of 0, 26.1, 45.6, 60.0, and 70.5° for An, Af/Aa, Bf/Ba, Cf/Ca, and Df/Da, respectively. The instantaneous displacement in the along-track direction between the Df and Da views is about 2800 km (see Fig. 2), and it takes about 7 min for a ground target to be observed by all nine cameras.

Each camera uses four charge coupled device (CCD) line arrays parallel in a single focal plane. The line array contains 1504 photoactive pixels, each $21 \times 18 \mu\text{m}$. Each line array is filtered to provide one of four MISR spectral bands. The spectral band shapes are approximately Gaussian and centered at 446, 558, 672, and 866 nm. Because of the physical displacement of the four line arrays within the focal plane of each camera, there is an along-track displacement in the

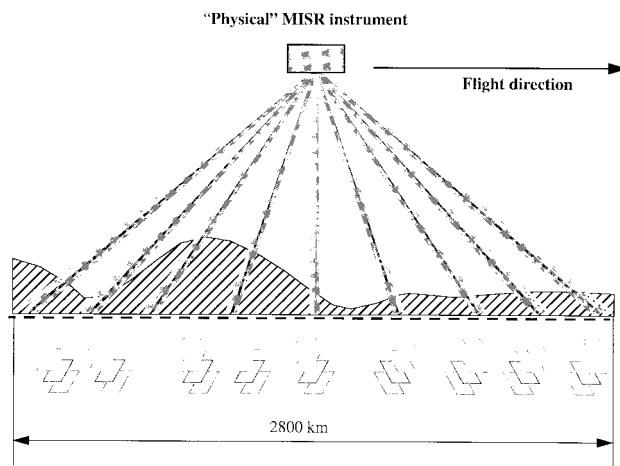


Fig. 2. MISR imaging event.

earth views at the four spectral bands. This must be removed during ground data processing.

The cross-track instantaneous field-of-view (IFOV) and sample spacing of each pixel is 275 m for all of the off-nadir cameras and 250 m for the nadir camera. In order to simplify manufacturing, the same optical design is used for nadir and Af/Aa off-nadir cameras, resulting in slightly different cross-

track IFOV's. Along-track IFOV's depend on view angle, ranging from 250 m in the nadir to 707 m at the most oblique angle. Sample spacing in the along-track direction is 275 m in all cameras.

In order to find the geolocation corresponding to a pixel's field-of-view, the pixel pointing direction is expressed in the geocentric coordinates system, as follows:

$$\hat{\rho} = T_1 \hat{r}_{scs} \quad (1)$$

where \hat{r}_{scs} is the pixel pointing direction relative to the spacecraft coordinate system (SCS). The vector \hat{r}_{scs} is defined by the observable image coordinates and the set of constants that represent the instrument interior orientation parameters and transformation between the instrument and spacecraft coordinate axes. T_1 , defined by the ephemeris and attitude data at the time of imaging, represents the transformation between the spacecraft and geocentric coordinate system. Equation (1) is an often used photogrammetric model [12] suitable for various image-ground point determinations required for satellite-based imagery.

III. PHOTOGRAMMETRY-BASED DATA PRODUCTS

In order to satisfy coregistration and geolocation requirements, the multiangle multispectral data are processed to a common map projection. We have selected Space Oblique Mercator [13] as the reference map projection grid because it is designed for continuous mapping of satellite imagery. The ground resolution of the map grid is 275 m. We define this segment of ground processing as "georectification" and the derived product as the Georectified Radiance Product.

There are two basic parameters in the Georectified Radiance Product, depending on the definition of the reflecting surface: a) ellipsoid-projected radiance and b) terrain-projected radiance. The ellipsoid-projected radiance is referenced to the surface of the WGS84 ellipsoid (no terrain elevation included), and the terrain-projected radiance is referenced to the same datum, including a digital elevation model over land and inland water.

An ideal instrument would collect each angular view for the terrain-projected and ellipsoid-projected radiance parameters for a ground point at the same instant, giving the radiance for each band and angle for that ground point (the so-called "virtual" MISR instrument). Of course, the real MISR instrument cannot do this. It is the job of geometric processing to produce data as if it were collected by the "virtual" MISR (compare Figs. 2–4).

The spatial horizontal accuracy goal associated with these products and required by the science algorithms is an uncertainty better than ± 275 m at a confidence level of 95%. Obviously, this kind of accuracy requires knowledge of a digital elevation model and removal of the displacement due to relief. In addition, the accuracy specifications for the supplied spacecraft navigation and attitude data suggest the possibility of horizontal errors of about 2 km in the most oblique cameras. Section IV discusses the algorithms that account for the displacement due to the topography and errors in

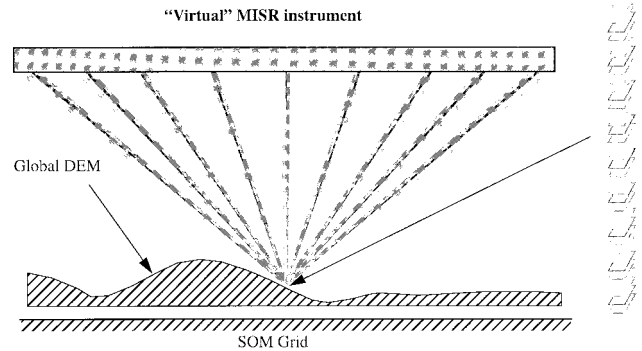


Fig. 3. Terrain-projected radiance product: output from a "virtual" MISR.

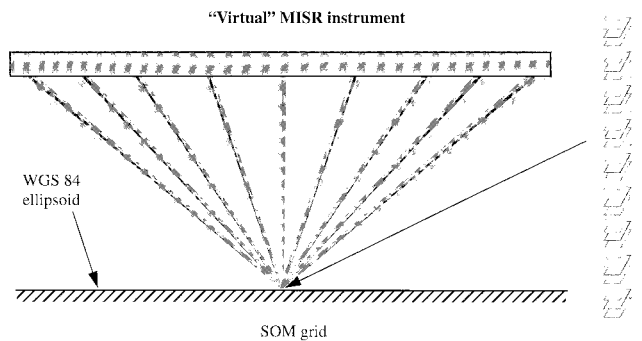


Fig. 4. Ellipsoid-projected radiance product: output from a "virtual" MISR.

the spacecraft navigation data prior to the resampling of the acquired MISR imagery to the map grid.

In addition to the Georectified Radiance Product, a photogrammetry-based algorithm is used to derive cloud height parameters for the Level-2 top-of-the-atmosphere (TOA)/cloud product. MISR multiple views obtained from satellite altitude over a wide angular range provide the ability to separate the effects of cloud wind displacement from cloud height. In particular, a reference projection level known as the Reflecting Level Reference Altitude will be established using a stereophotogrammetric algorithm. This is defined to be the level found by matching features [11] with the greatest contrast in the near-nadir viewing directions. Physically, this corresponds to the main reflecting layer, which will typically be either the tops of bright clouds or, under atmospheric conditions corresponding to clear skies or thin cloud, the surface of the earth.

IV. OVERVIEW OF PHOTOGRAMMETRY-BASED PROCESSING

In response to the specific spatial accuracy requirements, together with the need for autonomous and continuous production capabilities, we adopted a processing strategy that partitions effort between the MISR Science Computing Facility, Jet Propulsion Laboratory, California Institute of Technology, Pasadena, and the EOS Distributed Active Archive Center (DAAC), NASA Langley Research Center, Hampton, VA, in a way that minimizes the amount of processing required at the latter location. Activities at the Science Computing Facility

lower the computational need at the DAAC by precalculating certain data sets early in the mission and staging them for ongoing use, in a manner that avoids much calculation during routine ground processing. These data sets include the camera geometric model, reference orbit imagery, and projection parameters (described in Section V). Their preparation need occur only a few times during the mission, but it is highly computationally intensive, involving techniques such as ray casting and the matching of imagery from different camera angles. Consequently, routine processing of MISR data at the DAAC, the characteristics of which are dominated by the very high data volume, is optimized to require only the less computationally intensive work, such as matching of imagery from the same camera angle (not different camera angles) with no need for ray casting nor a high-resolution digital elevation model. Fig. 5 illustrates partitioning of photogrammetric operations between the Science Computing Facility and the DAAC.

From the entire MISR production system, three segments can be singled out as photogrammetric in nature. These are 1) inflight geometric calibration, 2) georectification, and 3) cloud height retrieval.

Inflight geometric calibration is designed in response to specific requirements for standard processing: 1) balance between limited hardware resources, huge data volume, and processing and 2) autonomous and ongoing production throughout the mission. The inflight geometric calibration operations are not part of standard processing. Instead, they will occur at the Science Computing Facility with the objective of producing a deometric calibration data set during the first six–eight months of the mission. This data set is used as an input to georectification processing to reduce processing load and provide the best possible input to automatic image registration. To produce a good-quality geometric calibration data set requires precise determination of the cameras interior geometry as well as determination of the instrument exterior orientation, taking into account errors in the supplied navigation and attitude. For that purpose, photogrammetric techniques will be used, such as: 1) space resection, 2) simultaneous bundle adjustment, and 3) combined feature/area-based image matching.

Given the geometric calibration data set as an input, the georectification during standard processing is significantly simplified. In particular, the most challenging part of the georectification is the image-to-image registration between new MISR imagery and reference imagery prepared as part of inflight geometric calibration (see Section V-B). It is possible to have this process robust and fully autonomous due to the fact that registration will occur between images with the same viewing geometry. Essentially, an image point intersection algorithm is employed, as the backward projection based on the camera model and supplied navigation, to obtain an initial guess for the tie points to be used during registration [12]. Precise location of the tie points, prior to resampling, is obtained through least-square area-based matching. The terrain-projected radiance produced during georectification is used as the input to Level-2 aerosol/surface retrievals and cloud mask generation. Another part of the georectified product,

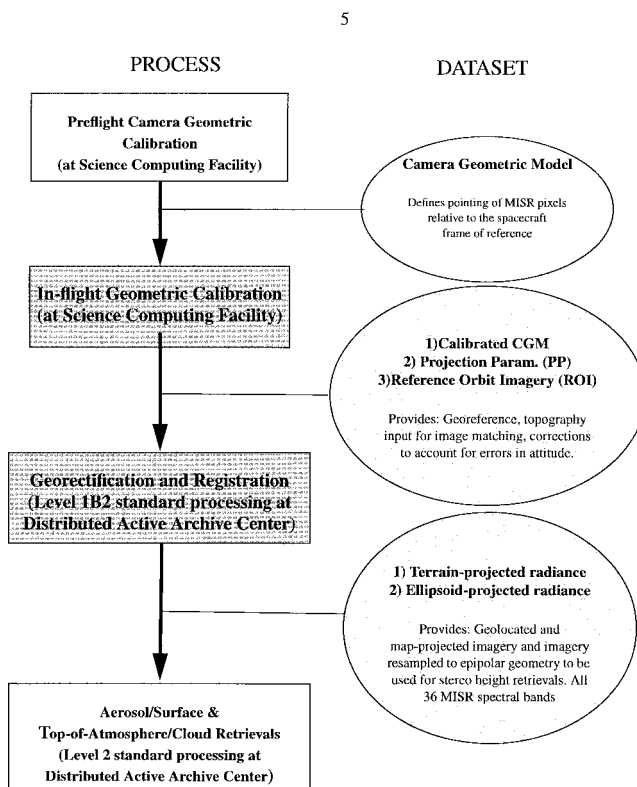


Fig. 5. Processes and data sets of the MISR production system related to algorithms based on photogrammetric methods.

ellipsoid-projected radiance, is used for Level-2 TOA/cloud stereoscopic retrievals.

The photogrammetric approach to cloud-top height retrieval is a singular problem if cloud motion is not known. In order to fully use the MISR image data to perform stereo retrieval of cloud-top heights, we must be able to separate the effects of cloud motion and cloud height in the image disparities. This has been proven mathematically to be possible under certain imaging conditions. The MISR instrument satisfies these conditions if we perform stereo matching and retrieval with the right combination of asymmetric MISR cameras.

V. INFLIGHT GEOMETRIC CALIBRATION

In order to give insight into photogrammetric algorithms used during inflight calibration, we first describe the geometric calibration data set resulting from this calibration. This data set consist of two major parts: 1) Camera Geometric Model and 2) Projection Parameters and Reference Orbit Imagery.

A. Camera Geometric Model

The Camera Geometric Model data set consists of a set of parameters that are used in a mathematical expression that gives the pointing direction of an arbitrary pixel. These parameters reflect geometries of the camera system and account for distortions (including temperature dependencies) from an ideal optical system [8]. There will be nine sets of parameters corresponding to the nine MISR cameras.

A mathematical expression relating line and sample (l, s) coordinates of a band in one of the MISR cameras to the vector \hat{r}_{scs} in SCS can be written as

$$\hat{r}_{scs} = T_{si} \cdot T_{ic} \cdot T_{cd} \cdot \begin{bmatrix} -(k + (l - INT(l + 0.5))d_x) \\ f \sum_{i=0}^5 \alpha_i (s - c_y)^i \\ f \end{bmatrix}. \quad (2)$$

where

| | |
|----------------------------------|--|
| T_{si} | rotation matrix function of the angles between the spacecraft and instrument coordinate systems; |
| T_{ic} | rotation matrix function of the angles between the instrument and camera coordinate systems; |
| T_{cd} | rotation matrix function of the angles between camera and detector coordinate systems; |
| k | separation of the particular band from the intersection of z the axis with focal plane (see Fig. 6); |
| c_y | pixel number (i.e., boresight pixel) corresponding to the x axis ($y = 0$); |
| d_x | detector pitch in x direction; |
| f | effective focal length; |
| $\alpha_i, i = 0, 1, 2, 3, 4, 5$ | coefficients of a fifth-order polynomial to account for the nonlinear distortions of the field angle in the cross-track direction. |

Equation (2) is the explicit way of defining the pointing direction of an individual pixel relative to the appropriate coordinate system. The number and type of parameters depend on the individual sensor characteristics. In photogrammetric terminology, MISR Camera Geometric Model data are called the "interior orientation parameters." Using the same terminology, the supplied navigation data defines what are called "exterior orientation parameters." Thus, the Camera Geometric Model in conjunction with the supplied navigation data will provide the pointing vector of an arbitrary pixel, relative to the earth-fixed, earth-centered coordinate system. This pointing vector is the fundamental information used during standard georectification for both the terrain-projected and ellipsoid-projected radiances.

B. Projection Parameters and Reference Orbit Imagery

The full set of Reference Orbit Imagery (ROI) consists of selected cloud-free MISR imagery mosaicked and stored in the 233 files corresponding to the 233 orbit paths of the EOS-AM1 spacecraft. Organized similarly into 233 files are the Projection Parameters (PP), which are produced offline using rigorous photogrammetric reduction methods. The PP files provide geolocation information for acquired MISR imagery on a pixel-by-pixel basis. This geolocation information is referenced to a selected Space Oblique Mercator map projection grid. The process of creating ROI and PP files is similar to the regular orthorectification of time-dependent sensor imagery. The major differences are that 1) acquired

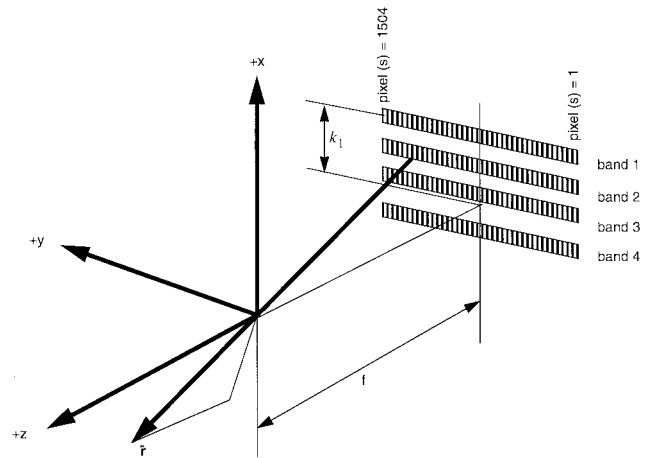


Fig. 6. Detector Coordinate System of the Camera Geometric Model. The x -axis is defined to be perpendicular to the long axis of the detector arrays. The y -axis is parallel to the long axis and positive in the westward direction during a descending pass. The z -axis is the cross product of x with y , forming a right-handed coordinate system. The figure shows that the focal plane is located at $z = -f$, where f is the effective focal length of the particular camera.

imagery is geolocated but not resampled and 2) a global digital elevation model of sufficient resolution is available for MISR's internal use. A simultaneous bundle adjustment utilizing multiangle imagery and ground control information (global digital elevation model and ground control point chips) is used to model errors in the navigation and attitude data for a single set of ROI, prior to geolocation.

The coupled PP and ROI files provide two major benefits to the standard georectification processing. First, expensive computation required to account for topographic displacement will be performed only once, offline during calibration. The obtained information will be saved in a file and utilized during online processing throughout the mission. This is possible because of the small orbit-to-orbit variations at the same location within an orbit path, adding relatively small changes to the topographic displacements that can be accounted for in a separate process during georectification. Second, unresampled but geolocated MISR imagery will be used as ground control information. The idea is that MISR imagery with close to the same viewing geometry will provide a high success rate during least-square area-based image matching performed by standard processing during image-to-image registration.

C. Calibration Algorithm

This algorithm consists of two parts: part one focuses on the removal of distortions from the Camera Geometric Model measured on the ground. These distortions result from the deformations of mechanical connections between the cameras, optical bench, and the spacecraft platform, caused by launch and gravity release of the camera system. Part two focuses on the production of the specific information useful for the routine removal of the navigation and attitude errors and distortions due to the surface topography. This information is stored in the PP's and ROI files, which along with the Camera Geometric Model, make up the Geometric Calibration Data set that is

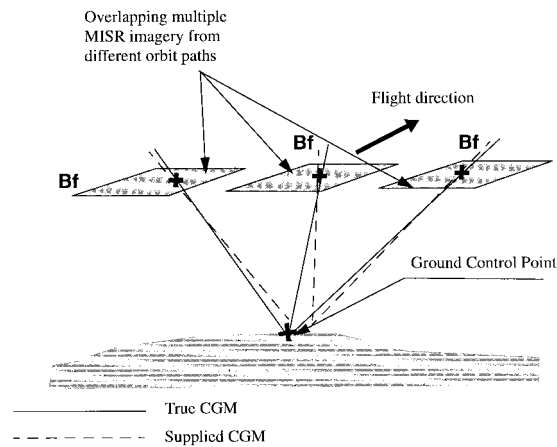


Fig. 7. Inflight camera geometric model calibration.

used as the input to the Level-1B2 georectification standard processing algorithm.

1) *Inflight Camera Geometric Model Calibration*: Some of the parameters of the camera model characterized during preflight ground calibration [8] must be verified on orbit. The exact subset of parameters to be recalibrated is still to be determined. The calibration algorithm will make use of ground control points (GCP's), and it will focus on the recalibration of each camera individually. The idea is to isolate static and systematic (e.g., temperature dependent) errors of the individual cameras from the errors reported in the navigation data. This is possible by having a large number of observations by a single camera of well-defined and well-distributed ground targets or GCP's (Fig. 7). Area-based image matching is used for automatic identification of GCP's.

A mathematical expression used to describe the ray between a ground point and the image of that point, as seen by an MISR camera, is used as the model for the least-squares estimation [10] of certain camera model parameters, i.e., space resection. A large number of observations and good distribution of GCP's are needed so that the effects of errors in the navigation data on the estimation of camera model parameters can be fully minimized. In that regard, it should be pointed out that a single GCP will be seen multiple times from a single camera during a 16-day period. This is important because it significantly increases the number of observations and, at the same time, provides a good distribution of ground control points across a camera field-of-view.

2) *Creation of PP's and ROI*: The calibrated Camera Geometric Model may not be sufficient to provide a product of the desired geolocation and registration accuracy. After applying the calibrated camera model, two types of errors remain significant: 1) errors in the navigation data and 2) displacements due to the surface topography. The following steps will be conducted at the MISR Science Computing Facility to remove the effects of those errors and create the PP and ROI files.

a) *Forward Projection*: A pixel in the map grid might not be seen by a particular MISR view angle because it is topographically obscured by the surrounding terrain (see Fig. 8).

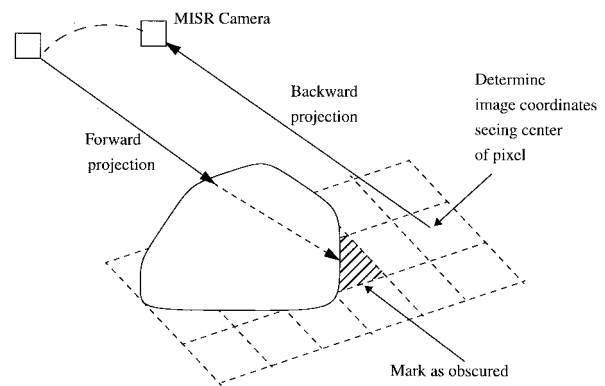


Fig. 8. Backward/forward projection.

To determine this, a ray casting algorithm is used, also referred to as a forward projection. A nominal set of navigation data and camera viewing geometry is used. Subpixeling (i.e., ray casting more than one ray for a single pixel) is performed to give a nominal ground pixel size of the resolution of the digital elevation model used to describe the terrain (i.e., about 100 m). If any one of the subpixels of a map grid pixel is not seen by an MISR camera, the whole map grid pixel is marked as obscured at that camera angle. The information about which map pixels are obscured is stored in the PP file for use by the georectification algorithm.

b) *Backward Projection*: After determining which map grid pixels are obscured, the location in the MISR imagery where the center of each map grid pixel is seen is determined for each camera angle. This is done by using a modified image point intersection algorithm, described in more detail in Section VI-B. The same nominal set of navigation data and camera viewing geometry, as in Step a), is used. This information is stored in the PP files for use by the georectification algorithm.

After performing steps a) and b), the PP files contain the information needed to resample MISR imagery acquired with nominal navigation data and camera viewing geometry. Of course, we do not expect to acquire image data with navigation data and camera viewing geometry identical to the nominal set. Real data will contain perturbations in the spacecraft position and attitude. The point is that the problem of resampling real MISR imagery to the map grid has been reduced to the problem of accounting for differences between the real navigation data and camera viewing geometry and the nominal set used to produce the PP. The PP then gives the remaining information about how to perform the map projection, once the differences with the nominal case are taken into account.

c) *Adjustment*: A "simultaneous bundle adjustment" (a least-square data estimation technique) constrained by a relatively high-resolution digital elevation model is used to improve the accuracy of the navigation data later used to produce ROI consistent with the set of PP obtained by using nominal orbit data.

The simultaneous bundle adjustment takes advantage of the following MISR characteristics: 1) at a single instant of time, MISR "sees" nine different, widely separated, targets

on the ground and 2) a single location on the ground is seen at nine different instants of time. If the errors in the navigation data are modeled as time dependent, it is possible to write a mathematical model that will utilize known MISR characteristics and improve the accuracy of the navigation data.

This model is certainly good for improving relative accuracy (during a time period) of the navigation data. In order to obtain absolute accuracy (i.e., relative to a fixed ground coordinate system), additional ground control information is needed. For that purpose, in addition to already available GCP's, a high-resolution digital elevation model is included as a good constraint to the adjustment.

Due to the fact that GCP's have to be manually collected and sparsely distributed, an automatic and robust tie-point identification algorithm is designed to provide well-distributed tie-points for the simultaneous bundle adjustment. A tie-point refers to the conjugate image feature locations of the same ground point across multiple images viewed from various angles. Based on initial conjugate image locations determined using the knowledge of MISR navigation data, interest point features are detected independently on all nine local conjugate image patches extracted from MISR imagery [4]. A feature-based matching scheme, namely, consistent labeling with forward check [6], is used to match conjugate interest points as improved tie-points, compared to the original ones. An area-based matching algorithm is then used to accurately identify the final tie-point with an uncertainty of less than 0.2 pixel. The tie-point identification is a completely automated process without human intervention. A supporting method with a human operator in the loop will be used mostly for validation purposes and some infrequent occasions when improvement of the automatic detection of tie points is needed.

d) Reference Orbit Imagery: In order to determine the differences between real MISR data and the nominal navigation data and camera viewing geometry used to produce the PP, a data set called the ROI is produced. This data provides ground control that can be image matched to newly acquired MISR image data during the georectification process (see Section VI-C). The ROI is created by mosaicking MISR image data to maximize cloud-free regions. The image data are resampled to make it appear as if they were acquired using the nominal navigation data and camera viewing geometry used in the production of PP. This resampling is done by building an image-to-image transform (see Section VI-D) between the MISR image data and an image with nominal navigation data. The transform is built using improved navigation data generated in Step c).

VI. GEORECTIFICATION ALGORITHM

A. Overview

In the systematic georectification system, we make use of ancillary data sets, namely, a set of PP's and ROI, produced at the beginning of the mission. The major information implicitly contained in these data sets is error-free navigation and attitude data, georeference, and surface topography relative to the var-

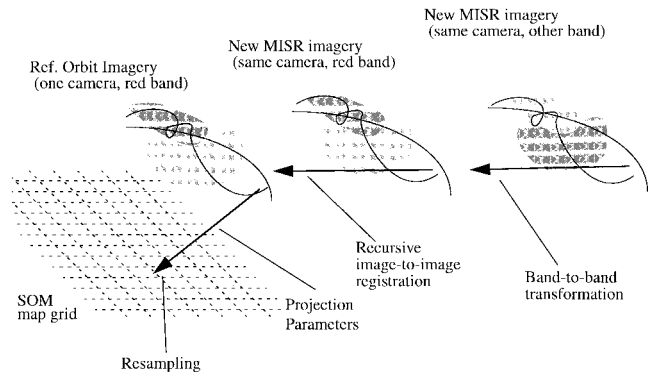


Fig. 9. Implementation of terrain-projection algorithm.

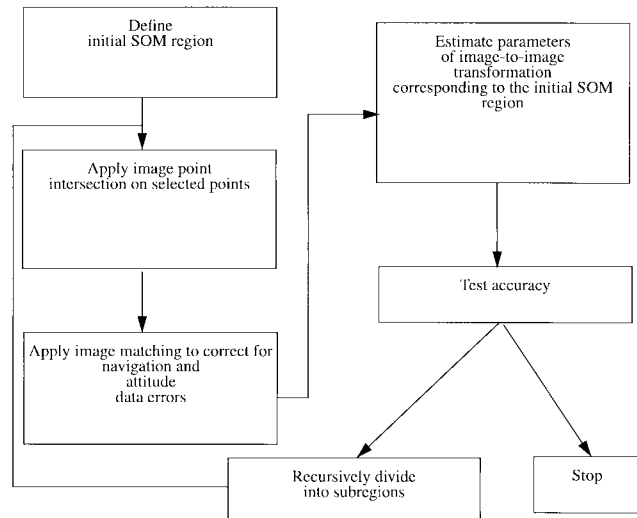


Fig. 10. Recursive image-to-image registration.

ious geometries of the nine MISR cameras. This information is routinely exploited through a hybrid image registration algorithm (see Fig. 9). In particular, the autonomous and continuous georectification is reduced to a recursive image registration between ROI and new MISR imagery, which consists of the following elements:

- 1) image point intersection: a backward projection function used to provide an initial location of the conjugate points [12];
- 2) image matching for the precise identification of the conjugate points;
- 3) transformation (mapping) function between two images.

The registration method is adaptive with regard to the character and size of misregistration to minimize the processing load. The adaptive nature of the algorithm is attained by recursively dividing images into subregions until the required registration accuracy is achieved (see Fig. 10). Initially, due to the pushbroom nature of the MISR cameras, subregions are rectangles extending over the image in the cross-track direction. The mapping function associated with a subregion is a modification of the affine transform, which includes known geometric characteristics of the MISR imaging event. Once

the mapping between the two images is established, the last processing step is the assignment of the appropriate radiance value to the grid point of the Space Oblique Mercator map. This is done using bilinear interpolation.

Additional techniques are required so that autonomous production runs are unaffected by less-than-perfect input data. Some of the more obvious examples are the presence of cloudy regions, water bodies, and deserts. These types of conditions significantly reduce the number of conjugate points available to determine the transformation function. In such cases, additional techniques must be implemented. In some cases, searching for cloud-free land in the local neighborhood may be sufficient. In other cases, where a large region of data is without conjugate points, use of information obtained through the registration of the closest subregion is applied. The idea is to correct for slowly varying parameters through the use of a Kalman filter built while processing previous subregions.

Also included in the algorithm is a blunder detection technique aimed at removing possible blunders coming from the image matching. This utilizes statistical results obtained from the least-square estimation of the transformation function.

B. Image Point Intersection

A rigorous ground-to-image projection is used to compute image coordinates of the initial tie points prior to image matching. It utilizes a well-known collinearity condition modified for MISR time-dependent imagery constrained by the equation that describes the spacecraft trajectory. It is obtained utilizing the ground point coordinates \hat{x} , the position of the sensor at time of imaging \hat{p} , and the pointing direction of the ray imaging the ground point [see (1)], all referenced to the geocentric coordinate system

$$\hat{x} = \hat{p} + \lambda \hat{p} \quad (3)$$

where λ is a scale factor. Using an iterative root-finding method, (3) can be solved for the image coordinate of the ground point. Initial input to the iterative solution is obtained from the PP file in conjunction with nominal orbit parameters.

C. Image Matching

An image matching technique has been chosen in order to 1) precisely locate tie points during image-to-image registration and 2) estimate the accuracy of the local image-to-image transformation. Our decision to use a combination of cross-correlation and least-square area-based image matching method [1] is based largely on two factors. First, the high sub-pixel accuracy of successful matches that can be achieved [5]. Second, MISR new and reference images with their minimal perspective changes between the two views will serve as very good input to the selected method. The sizes of the “target” and “search” windows are based on the expected errors in the supplied navigation and attitude data. For completeness, we give a mathematical description of the implemented area-based matching.

First, using the results from the image point intersection, the points from new and reference images are matched based

on a variation of the normalized cross-correlation, computed as follows:

$$C = \frac{\sigma_{\text{new,ref}} \cdot |\sigma_{\text{new,ref}}|}{\sigma_{\text{new}}^2 \cdot \sigma_{\text{ref}}^2} \quad (4)$$

where $\sigma_{\text{new,ref}}$ is the covariance between new and reference MISR image chips and $\sigma_{\text{new}}^2, \sigma_{\text{ref}}^2$ are the variances.

The results obtained by the cross-correlation method are improved to subpixel accuracy by least-square matching. In the least-square matching, the geometric and radiometric transformations between two image chips are estimated by minimizing certain functions between them. Let

$$\begin{aligned} x', y' & \text{ coordinates in the reference image;} \\ x'', y'' & \text{ coordinates in the new image.} \end{aligned}$$

Then the geometric relation is modeled by the affine transformation

$$\begin{aligned} x'' &= F_x(x', y') = a_0 + a_1 \cdot x' + a_2 \cdot y' \\ y'' &= F_y(x', y') = a_3 + a_4 \cdot x' + a_5 \cdot y'. \end{aligned} \quad (5)$$

Also, if

$$\begin{aligned} g' &= G'(x', y') + n'(x, y) \\ g'' &= G''(x'', y'') + n''(x'', y'') \end{aligned} \quad (6)$$

are the discrete radiance values for reference and new image, respectively, where G' and G'' are image functions, while n' and n'' are associated noise values, the radiometric relation is expressed as a two-parameter linear function

$$g' = F_r(g'') = k_0 + k_1 \cdot g''(F_x, F_y). \quad (7)$$

Through iterations using linearized form of (7), we solve for parameters a_i and k_i .

D. Image-to-Image Transformation

A polynomial form to be used for image-to-image transformation between new and reference imagery was derived by looking at the physical characteristics of a pushbroom camera. We built a model that describes how a scan line of the reference image maps to the new image. We then assumed that the mapping for nearby scan lines should be nearly identical. Although the model was derived for a single scan line, we apply it to a larger area (nominally 256 lines of data).

The physical aspects modeled include: 1) linear optics (i.e., we ignore the small nonlinearities in the camera optics), 2) earth curvature, and 3) effect of ground topography. The image geometry in terms of the sample coordinates was defined explicitly using simple trigonometry, pinhole camera model, and spherical earth model. The sample and line image disparities are then obtained by doing a series expansion and eliminating the insignificant higher order terms. This gives the following modification of the general affine transformation:

$$\begin{aligned} s_{\text{new}} &= k_{14}(l_{\text{ref}} - l_0) + k_{15}(s_{\text{ref}} - s_0) + k_{16}(s_{\text{ref}} - s_0)^2 \\ &\quad + k_{17}h_{\text{surface}} + k_{18} \end{aligned} \quad (8)$$

$$\begin{aligned} l_{\text{new}} &= k_{19}(l_{\text{ref}} - l_0) + k_{20}(s_{\text{ref}} - s_0) + k_{21}(s_{\text{ref}} - s_0)^2 \\ &\quad + k_{22}h_{\text{surface}} + k_{23} \end{aligned} \quad (9)$$

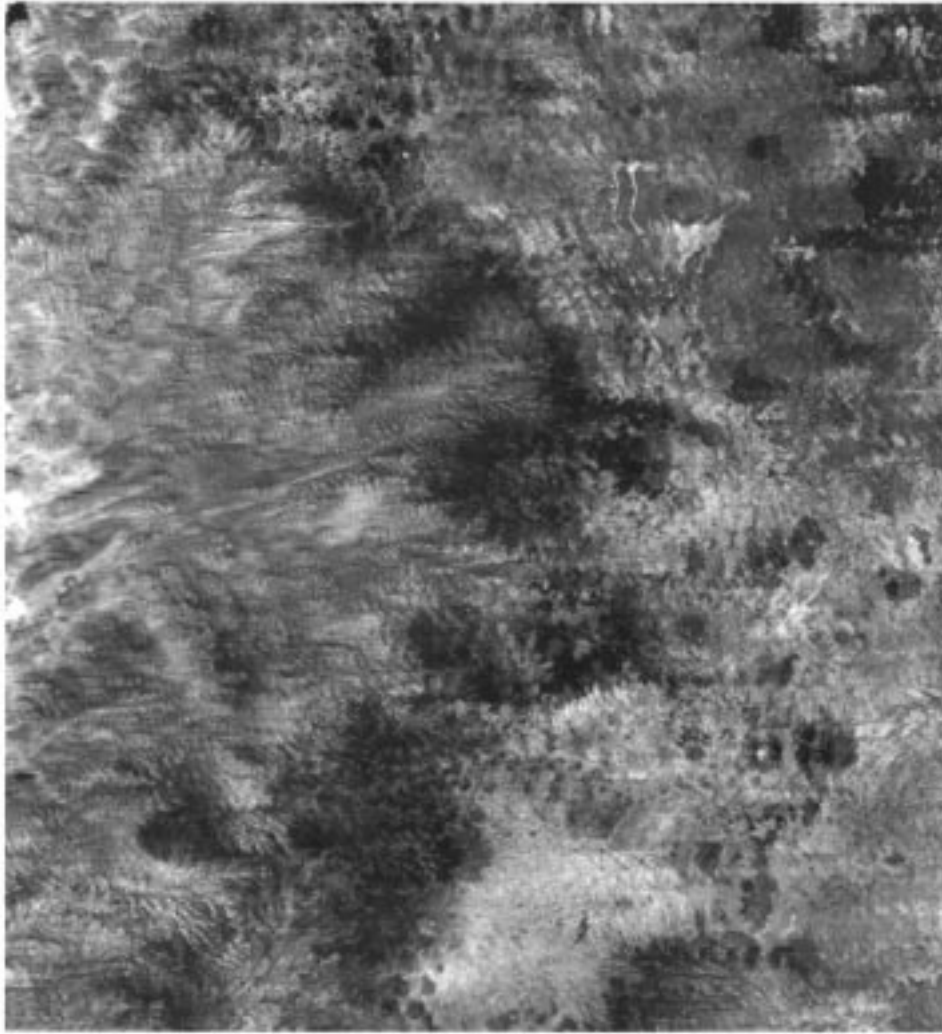


Fig. 11. Ellipsoid-projected red band data for A forward (Af) and C aft (Ca) cameras are superimposed to make this color composite. The Af camera image data are color-coded red and the Ca camera image data are color-coded blue and green to make a pseudocolor image suitable for stereo viewing with standard red and blue filter glasses. This shows the effect of the along-track parallax preserved in the ellipsoid-projected data, which are used for stereo-cloud height retrievals.

where l_0 and s_0 define the origin of an image coordinate system and $l_{\text{ref}}, s_{\text{ref}}, l_{\text{new}}, s_{\text{new}}$ are line and sample coordinates in new and reference images, respectively. The $k_{i,j}$ coefficients can be computed through the use of image-to-image tie points. Testing shows that the corrections we have derived to the affine model are important. The quadratic term at the edges of the swath can be as large as two pixels. However, the height term is usually small and, in the Beta version of the MISR software, it was dropped from the model.

We use this transform in the following manner.

- 1) Start with a region of imagery (nominally 256 lines, full swath).
- 2) Find well-distributed conjugate points in the reference and new imagery. This requires finding points in areas where image matching can be performed (e.g., cloud-free land).
- 3) Use conjugate points to determine the coefficients in (8) and (9) by doing a least-squares fit.
- 4) Find another set of conjugate points to use as check points. Compare the prediction of the location of the

conjugate points in the new image obtained by (8) and (9) to the actual location. If they are within the allowed tolerances (e.g., 1/2 pixel), we are done. Otherwise, break the region into two smaller pieces, and repeat the process for each of the smaller pieces.

E. Blunder Detection

A blunder detection function was implemented to prevent low accuracy and extra subgridding effort caused by the appearance of blunders from image matching. The least-square fit of image-to-image transform can be represented by a general observation equation

$$v = Ax - y \quad (10)$$

where the observation y is a set of random variables $y \sim (Y, \sigma_0^2 Q_{yy})$, $Y = Ax$ is the true value of the observation, σ_0 is the reference standard deviation of the observation, Q_{yy} is the weight matrix, x is the set of unknown parameters, A is the design matrix relating x to y , and v is the residual

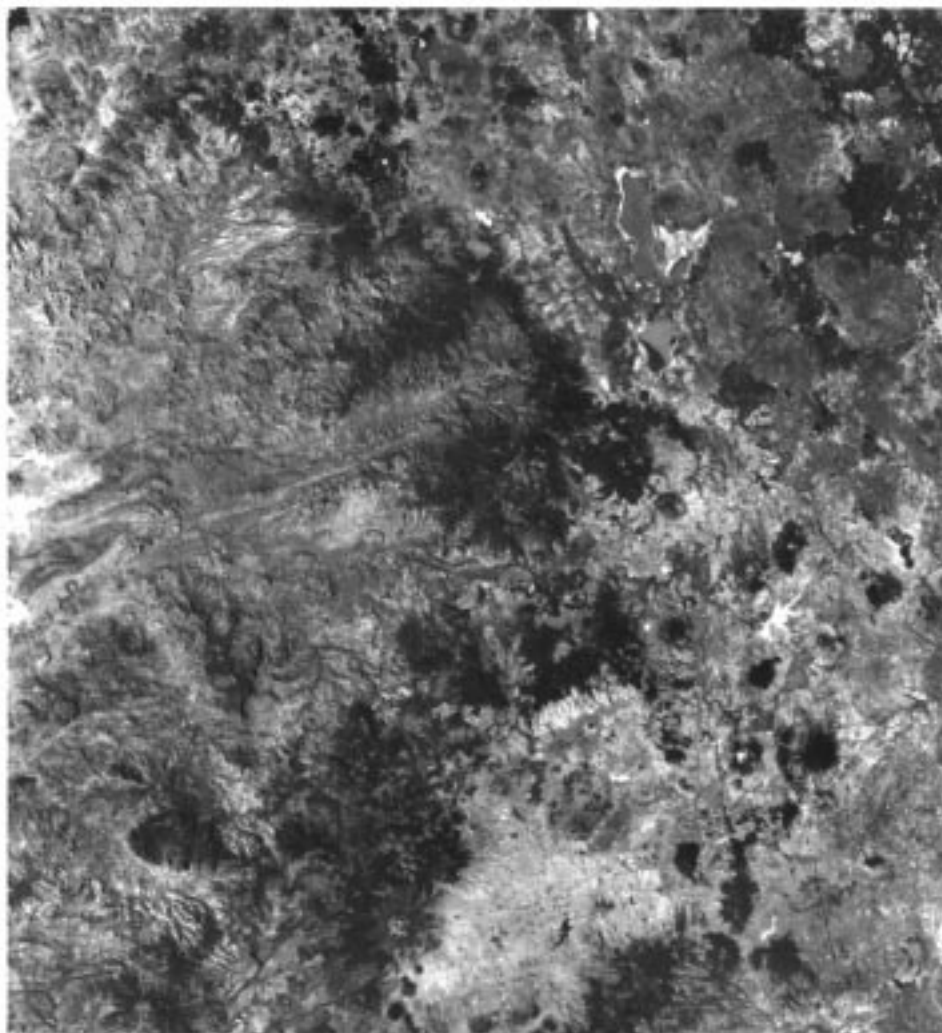


Fig. 12. Terrain-projected red band data for A forward (Af) and C aft (Ca) cameras are superimposed to make this color composite. The Af camera image data are color-coded red and the Ca camera image data are color-coded blue and green to make a pseudocolor image. Due to the terrain projection, parallax is removed and overlaid data appear like a single orthorectified image. The small regions of red pixels represent topographic obstructions to the viewing angle (see Section V-C). A significant portion of these pixels cannot be imaged by either Af or CA cameras.

$v = y - Y$. The best estimated least-square solution to the above linear system is to minimize $\phi = v^T W v$, where weight matrix $W = Q^{-1}$. This minimum principal easily leads to a normal equation $\tilde{x} = Q_{xx} A^T W_{yy} y$, where the cofactor matrix of the estimated unknown parameters is $Q_{xx} = (A^T W_{yy} A)^{-1}$. The residual vector and its cofactor matrix are then related by the following equation as:

$$v = A\tilde{x} - y = (A Q_{xx} A^T W_{yy} - I)y = -(Q_{vv} W_{yy})y. \quad (11)$$

Equation (11) indicates how the errors of one or more of the observations (Δy) influence the residuals. This relation can be written as $v = -(Q_{vv} W_{yy})\Delta y$. It shows that the cofactor matrix of the residual Q_{vv} and the observation weight matrix P_{yy} are the key to the relationship of the observation-errors or blunders Δy to their corresponding residual. In case of equal weight, a large diagonal value of Q_{vv} means that an observation error is translated to the corresponding residual, a small diagonal value diffuses the observation error. The

off-diagonal value of Q_{vv} does the opposite. The fact of a large off-diagonal value can pass an observation error to other residual than the corresponding one is caused by the high correlation among observations. This effect can be minimized by good configuration of our control point distribution.

Assume there is no gross error in an observation but only a random error which follows a normal distribution. Accordingly, the residuals will also follow a normal distribution with mean expectation of zero and a variance of σ_v^2 . The mean error of residual v_i can be represented as $\sigma_{v_i} = \sigma_0 \sqrt{(Q_{vv})_{ii}}$. Therefore, the accuracy of the residual v_i depends not only on the observation error, but also on the diagonal values of Q_{vv} . Obviously, the standardized residuals $\bar{v}_i = v_i / \sigma_{v_i}$ follow a standardized normal-distribution with expectation zero and variance one. The effect of diagonal value of Q_{vv} is reduced in this representation. The standardized residuals are ideal for statistical testing to detect blunders. However, statistical testing only works with few blunders and the removing of blunder is one at a fitting time and, therefore, called data snooping. If blunders exist during one data fitting, the

postestimated variance per unit weight $\hat{\sigma}_0 = \phi/r$ (r as the redundancy of the system) testifies that first, and the test to the standardized residual instead of residual can be used to point out the causing blunder.

F. Band-to-Band Transformation

The registration between the new MISR image and ROI imagery has been done using the red spectral band (Fig. 9) because of its characteristics relative to the image matching requirements. The imagery from the other three bands will be registered to the already registered and geolocated red band. This registration does not include image matching. Rather, the transformation between bands is defined by the interior orientation parameters of the geometric camera model. More details on this transformation can be found in [14].

VII. CONCLUSIONS

MISR photogrammetric data reduction is a unique and successful process. It provides effectively and precisely the georegistered information for geophysical and other scientific research usage. With the state-of-the-art photogrammetric techniques, we have been able to meet the georegistration requirement and multicamera coregistration requirements with our simulated test data [9]. Figs. 11 and 12 represent portions of the geometric product. They clearly show spatial accuracy of a multilayered map projection (Fig. 12) created for the terrain-projected radiance. Also, in Fig. 11, epipolar geometry and suitability of the ellipsoid-projected radiance for the stereo height retrievals are demonstrated.

ACKNOWLEDGMENT

The authors gratefully acknowledge the efforts of the MISR Principal Investigator, D. Diner, Co-Investigator, J. Muller, and the members of the Science Data System Team: E. Hansen, B. Rheingans, and S. Lewicki. Additional thanks are due to C. Bruegge and R. Korechoff for their efforts in MISR camera calibration.

REFERENCES

- [1] F. Ackermann, "Digital image correlation: Performance and potential application in photogrammetry," *Photogramm. Record*, vol. 11, p. 64, 1984.
- [2] D. Allison, M. J. Barnsley, P. Lewis N. Doble, and J.-P. Muller, "Precise geometric registration of ASAS airborne data for land surface BRDF studies," in *Proc. IGARSS*, 1994, vol. 3, pp. 1655-1657.
- [3] D. J. Diner, J. C. Beckert, T. H. Reilly, C. J. Bruegge, J. E. Conel, R. A. Kahn, J. V. Martonchik, T. P. Ackerman, R. Davis, S. A. W. Gerstl, H. R. Gordon, J.-P. Muller, R. B. Myneni, P. J. Sellers, B. Pinty, and M. M. Verstraete, "Multi-angle Imaging SpectroRadiometer (MISR) instrument description and experiment overview," this issue, pp. 1072-1087.
- [4] W. Forstner, "A fast operator for detection and precise location of distinct points, corners and centers of circular features," in *Proc. ISPRS Intercommission Workshop*, Interlaken, Switzerland, 1987.
- [5] ———, "On the geometric precision of digital correlation," in *Proc. ISPRS Int. Arch. Photogramm.*, Commission III, Helsinki, Finland, vol. XXIV, 1980.
- [6] R. Haralick and L. Shapiro, *Computer and Robot Vision*. New York: Addison-Wesley, 1993.
- [7] S. Herrick, *Astrodynamics*. New York: Van Nostrand Reinhold, 1971.
- [8] R. P. Korechoff, V. M. Jovanovic, E. B. Hochberg, D. M. Kirby, and C. A. Sepulveda, "Distortion calibration of the MISR linear detector arrays," in *Proc. SPIE*, Denver, CO, Aug. 1996, vol. 2820-19.

- [9] S. A. Lewicki, M. M. Smyth, V. M. Jovanovic, and E. G. Hansen, "A simulation of EOS MISR data and geometric processing for the prototyping of the MISR ground data system," in *Proc. IGARSS*, 1994, vol. 3, pp. 1543-1545.
- [10] E. M. Mikhail, *Observations and Least Square*. New York: Harper & Row, 1976.
- [11] J.-P. Muller, A. Mandanayake, R. Davis, and C. Moroney, "A comparison of stereo matching techniques for global cloud-top height retrieval from ATSR and MISR," *J. Geophys. Res.*, to be published.
- [12] F. C. Paderes, E. M. Mikhail, and J. A. Fagerman, "Batch and on-line evaluation of stereo spot imagery," in *Proc. ASPRS*, 1989, vol. 3.
- [13] J. P. Snyder, "Map projection—A working manual," United States Government Printing Office, Washington, DC, United States Geological Survey Professional Paper 1395, 1987.
- [14] J. Zong, V. M. Jovanovic, and M. M. Smyth, "MISR band-to-band registration," in *Proc. SPIE*, Denver, CO, Aug. 1996, vol. 2818-28.



Veljko M. Jovanovic received the M.Sc. degree in photogrammetry from Purdue University, West Lafayette, IN, in 1991.

He was with Intergraph Corporation, Huntsville, AL, from 1992 to 1993, where he was involved in the development of the first generation of the digital photogrammetric workstation. He joined the Jet Propulsion Laboratory, California Institute of Technology, Pasadena, in 1993, where he is presently a Member of the Technical Staff in the Science Data Processing Section. His interests are mainly directed toward the development of systems for automated digital mapping, image exploitation and analysis, and instrument geometric calibration. He is currently a Senior Photogrammetry Engineer for the Multi-angle Imaging SpectroRadiometer Project, for which he oversees activities related to the georectification functions of the science data processing system.



Michael M. Smyth received the B.S. degree in physics with honors from the California Institute of Technology, Pasadena, in 1990 and the M.S. degree in physics from Cornell University, Ithaca, NY, in 1993.

He has been with the Jet Propulsion Laboratory, California Institute of Technology, since 1993 and is currently a Member of the Science and Instrument Software Systems Group. He is currently working on the geometric calibration and registration software for the Multi-angle Imaging SpectroRadiometer (MISR) as well as the airborne counterpart, AirMISR.



Jia Zong received the B.S. degree in physics from the Nankai University, Tianjin, China, in 1984, the M.S. degree in physics from Southern Illinois University, in 1989, and the M.S. degree in photogrammetry from The Ohio State University, Columbus, in 1993.

She has been with the Jet Propulsion Laboratory, California Institute of Technology, Pasadena, since 1994, where she is a Member of the Information Science Staff. Currently, she is the Photogrammetry Engineer for the Multi-angle Imaging SpectroRadiometer (MISR) Project and is working on MISR geometric calibration and image processing algorithm design and validation.



Robert Ando received the B.S. degree in mechanical engineering from Duke University, Durham, NC, in 1973 and the M.S. degree in oceanography from Scripps Institution of Oceanography, La Jolla, CA, in 1978.

He has been with the Jet Propulsion Laboratory, California Institute of Technology, Pasadena, since 1996, creating realistic simulated data for testing Multi-angle Imaging SpectroRadiometer (MISR) software and providing software integration and test support.



Graham W. Bothwell received the B.Eng. degree in electronics from the University of Queensland, Brisbane, Australia, in 1967.

He was with NASA's Deep Space Station, Canberra, Australia, from 1967 to 1968. From 1969 to 1985, he was with the Anglo-Australian Observatory, Sydney, Australia, where he was involved in computing and electronics development in support of construction and subsequently operation of the 4-m telescope, becoming Head of Computing. He has been with the Jet Propulsion Laboratory (JPL), California Institute of Technology, Pasadena, since 1985, initially as Supervisor of a group developing image processing software for JPL's planetary program. Since 1988, he has worked with various projects associated with NASA's Earth Observing System, leading to a group involved in airborne remote sensing, ground system development, instrument data processing, and mission operations. He is currently Science Data System Manager for the Multi-angle Imaging SpectroRadiometer Project.